PAPER

Check for updates

Effective colloidal emulsion droplet regulation in flow-focusing glass capillary microfluidic device *via* collection tube variation

Tianyi Jiang, [ID] *[a] Hao Wu,*[ab] Shuofu Liu,[a] Hui Yan*[a] and Hongyuan Jiang[a]

Colloidal emulsion droplets, created using glass capillary microfluidic devices, have been found in a myriad of applications, serving as subtle microcarriers, delicate templates, *etc.* To meet the objective requirements under varying circumstances, it is crucial to efficiently control the morphology and dimensions of the droplets on demand. The glass capillary collection tube is a crucial component of the flow-focusing microfluidic system due to its close association with the geometrical confinement of the multiphasic flow. However, there are currently no guidelines for the design of the morphology and dimensions of the glass capillary collection tube, which shall result in a delay in assessing serviceability until after the microfluidic device is prepared, thereby causing a loss of time and effort. Herein, an experimental study was conducted to investigate the effect of the geometrical characteristics of glass capillary collection tubes on the production of colloidal emulsion droplets. After characterizing the generated colloidal emulsion droplets, it was found that the geometrical variations of the glass capillary collection tube resulted in numerical disparities of droplets due to different degrees of flow-focusing effects. The stronger flow-focusing effect produced smaller droplets at a higher frequency, and the dimensional variation of colloidal emulsion droplets was more responsive to varying flow rates. Furthermore, the transformation from colloidal single-core double-emulsion droplets to multi-core double-emulsion droplets also changed with the flow rate due to the glass capillary collection tube morphology-determined varying flow-focusing effect. These experimental findings can offer qualitative guidance for the design of glass capillary microfluidic devices in the preliminary stage, thus facilitating the smooth production of desired colloidal emulsion droplets.

1. Introduction

Colloidal emulsion droplets derived from microfluidic technology have emerged and served as delicate carriers and fundamental templates in a myriad of applications ranging from chemical analysis,[1–7] biomedical engineering,[8–14] and materials synthesis,[15–22] to the cosmetic industry,[23–26] *etc.* The innate small-volume endows the colloidal emulsion droplets with a series of advantages including a high surface aspect ratio, trace amount of reagent consumption, ultra-fast heat, and mass transfer as well as pronounced interfacial effects, which has laid a solid foundation for their practical usage.[27–29] However, for higher-end scenarios with stringent requirements, the degree of overall monodispersity as well as on-demand accurate morphology and dimension regulation are of vital importance during the generation process of colloidal emulsion droplets.

Generally, droplets are derived from fluid instability under the multiphasic circumstance, where the viscous shear force usually plays a dominant role in discretizing the continuous fluid stream. However, it should also be noted that the underlying rules of the droplet breaking-up phenomenon are rather complicated, where multiple physical factors should be taken into account, such as the interfacial tension, viscous and inertial forces, external inputs, boundary conditions, and so forth.[30–35] It is the synergistic effect of these factors that jointly determines the specific dynamic generation procedure within the multiphase fluid system. Based on the dynamic morphology of droplets during the generation process, the fluid mode can be classified into five categories, *i.e.*, squeezing, dripping, jetting, tip-multi-breaking, and tip-streaming.[36] In order to aid quantitative identification, real-time systems for image acquisition and characterization are generally introduced, which typically include data acquisition, transmission, and analysis modules. The *in situ* generation procedure of colloid emulsion droplets can be recorded by the built-in high-speed camera in the optical microscope and relevant data is then transmitted and stored by the supporting software in the connected computer. Subsequently, statistical analysis can be performed by examining

[a]School of Mechatronics Engineering, Harbin Institute of Technology, West Da-Zhi Street 92, Harbin, Heilongjiang, PR China 150001. E-mail: jty_hit@hit.edu.cn; whaohit@hit.edu.cn; yanhui@hit.edu.cn

[b]Department of Mechanical Engineering, City University of Hong Kong, Kowloon, Hong Kong SAR, PR China 999077

each frame using professional image processing software, such as Image J. To distinguish between fluid modes, dimensionless numbers, such as the Reynold number, Capillary number, Weber number, and Bond number, are used to describe the relative magnitude between each pair of physical quantities. Without the introduction of external fields, the physical parameters of interfacial tension, viscosity, density, and gravitational factors are predefined by the selection of each phase fluid and the ambient experimental environment. Thus, the direct regulation of fluid flow can act as the most straightforward way to realize the free switch among each droplet generation mode by influencing the inertial force and viscous force, which have already been reported by numerous scholars worldwide.[37–42] In addition, the configuration and dimension of the microfluidic device also play a critical role in the regulation of colloidal emulsion droplets as the channel geometry is directly associated with the spatial confinement that provides the boundary conditions for the microflow system. To date, microfluidic devices prepared by the sequential assembly of glass capillary tubes have been widely adopted due to the innate advantages of easy to process and integration, high throughput yield with fine droplet monodispersity, well resistance to organic solvents, *etc.*[43–50] Two basic geometrical forms, known as the co-flow and flow-focusing configurations, are widely utilized for the generation of colloidal emulsion droplets, in which the introduction of a glass capillary collection tube with a smaller orifice dimension in the flow-focusing configuration can effectively reduce the dimension of the generated colloidal emulsion droplets compared to the co-flow counterpart, which is more favorable for practical applications, especially for the preparation of complex higher-order emulsions.[51–55] However, till now, there is still a lack of standards and specifications for the design of the glass capillary collection tube in terms of both morphology and dimension, previous experiments prevalently adopted a conical morphology, and the corresponding dimensions were largely set with reference to personal experience. As a result, the only judgment to verify the availability of a prepared microfluidic device is to check whether the desired colloidal emulsion droplets can be generated. This hysteresis can inevitably bring about a waste of time and effort, drastically reducing the working efficiency. Moreover, there are few pieces of literature have systematically discussed the effect in terms of the morphology and dimension of the glass capillary collection tube in flow-focusing microfluidic devices upon the generation of colloidal emulsion droplets. Thus, it is imperative to experimentally clarify this issue, which is anticipated to provide qualitative instructions for the fabrication of flow-focusing glass capillary microfluidic devices at the preliminary stage.

Herein, we proposed a detailed experimental study to explore the morphological and dimensional influence of the glass capillary collection tube in flow-focusing microfluidic devices upon the generation of colloidal emulsion droplets. Assisted with precise microfabrication technology, three different morphologies, *i.e.*, the conical, the inner concave, and the parallel straight configurations, of the glass capillary collection tube with varying orifice dimensions were prepared to fabricate flow-focusing microfluidic devices. The single-emulsion, single-core double-emulsion, and multi-core double-emulsion droplets were then generated under a series of flow rate combinations and statistically analyzed regarding the droplet dimension and morphology. The numerical contrasting results were further correlated with the geometrical discrepancies of the glass capillary collection tubes and qualitative conclusions were drawn accordingly, which is expected to provide ponderable instructions for the design of flow-focusing glass capillary microfluidic devices.

2. Experimental section

2.1 Materials

Sigma-Aldrich supplied the water-soluble surfactant poly(vinyl alcohol) (PVA, 87–89% hydrolyzed, average $M_w = 13\,000$–$23\,000$) and the surface modification reagent trimethoxy(octadecyl) silane (OTS, average $M_w = 374.67$, technical grade). Dow Corning provided the silicone oil (PMX200) and the corresponding surfactant resin RSN-0749. The organic solvent toluene was obtained from Tianli Chemical Reagent Co. Ltd., which was used to dissolve the OTS in a mass ratio of 19 : 1 to prepare the surface wetting modification reagent. Deionized water produced by the Millipore Milli-Q system with a resistivity of 18.2 MΩ cm^{-1} was used. The experiments for generating colloidal oil-in-water (O/W) single-emulsion droplets and colloidal water-in-oil-in-water (W/O/W) double-emulsion droplets were conducted at room temperature (20 °C) and atmospheric pressure. The aqueous phase consisted of a 5%wt PVA solution, while the oil phase was made up of silicone oil with a viscosity of 50cst. It was important to note that the PVA solution was prepared in two stages. Firstly, PVA granules with the prescribed weight fraction were added in stages to deionized water and continuously stirred magnetically at 75 °C for 24 hours. A filtration process was implemented using filters with a filtration threshold of 0.45 μm to further purify the PVA solution. This was done to prevent potential blockage of the glass capillary tubes.

2.2 Preparation of the glass capillary microfluidic device

As shown in Fig. 2c, the glass capillary microfluidic device adopted a flow-focusing configuration with two inlets for fluid phases Q_1 and Q_2 on the left side, and one inlet for fluid phase Q_3 (for the preparation of colloidal W/O/W double-emulsion droplets) and an outlet for the as-prepared colloidal emulsion droplets on the right side. This configuration was analogous to previous report,[56] which involved inserting two circular glass capillary tubes (1B100-6, World Precision Instruments, Inc., outer diameter 1.03 mm) into one square glass capillary tube (810-9917, AIT Glass, Inc., inner diameter 1.05 mm). The circular glass capillary tube on the left was used as the incidence tube for fluid phase Q_1, while the circular glass capillary tube on the right was used as the collection tube for the generated colloidal emulsions. The flow paths of fluid phases Q_2 and Q_3 were the dimensional gaps between the incidence and collection tubes in relation to the square glass capillary tube on both sides. Before assembly, some preliminary treatments were

performed on the circular glass capillary tubes. These treatments included regulating the tip morphology and adjusting the dimensions, as well as modifying the surface wetting properties. Although most previous experiments used the conical tube for granted, the collection tubes used in this manuscript had three different morphologies: parallel straight, conical, and inner concave. These tubes were post-processed from commercial circular glass capillary tubes. The parallel straight collection tubes had dimensions of 300 μm, 500 μm, and 580 μm, achieved by nesting circular tubes with gradients of dimensions. The conical collection tubes were prepared using a micropipette puller (P-97, Sutter Instrument, Inc.) and a microforge (MF-900, Narishige, Tritech Research, Inc.). The circular glass capillary tube was split into two cylindrical counterparts with a small orifice size by the micropipette puller. The microforge was then used to adjust the orifice to the required size. All incidence glass capillary tubes in microfluidic devices were configured identically with a conical shape and an orifice dimension of 80 μm. The conical collection tubes had gradient dimensions of 150 μm, 250 μm, and 300 μm, respectively. To prepare the inner concave collection tube, heat the circular glass capillary tube evenly along the radial direction until the glass partially melts. Then, allow it to cool and solidify, which will cause a spontaneous necking and contraction process, transforming the circular glass capillary tube into the desired inner concave configuration. The inner concave collection tubes (with dimensions of 160 μm, 200 μm, and 300 μm) were created by precisely controlling the heating duration time. Secondly, for the preparation of colloidal emulsion droplets, it was imperative to make the oil phase flow path hydrophobic while leaving the other regions in their initial state. This was achieved by coating the inner or outer wall of the incidence conical glass capillary tube on the left side with OTS granules for the preparation of colloidal O/W single-emulsion droplets and W/O/W double-emulsion droplets, respectively. The prescribed glass surface was soaked in the prepared modification reagent for approximately 40 seconds. Specifically, the inner channel must remain ventilated while treating the outer wall. Afterward, transfer the conical glass capillary tubes to a hot plate and bake them at 160 °C to evaporate the toluene solution. The OTS particles that were initially dissolved would gradually precipitate and adhere to the corresponding surfaces, which would simultaneously reduce the glass capillary tube's transparency and improve its hydrophobicity. The specific assembly process was listed as follows after the preliminary treatments were completed.

(1) Cut out an approximately 30 mm long square glass tube and evenly smear photosensitive adhesive on one side of the tube. Then, stick it to the center of a rectangular glass substrate through UV exposure for 10 s.

(2) Immobilize the glass substrate onto the operating platform of the microscope with adhesive tapes. Afterward, insert the incidence and collection glass capillary tubes into the square one from both ends and manually align the coaxiality and axial distance under the horizon of the optical microscope.

(3) Two syringe needles were used as the inlets for fluid phases Q_2 and Q_3, which were fixed by epoxy adhesive onto the

glass substrate and thus wrapped the formed dimensional gaps of the glass capillary tubes. Thus, there were four outlets of the microfluidic device, including the two circular ends of the incidence and collection glass capillary tubes, as well as the two syringe needles, which were further connected to respective terminals with Teflon hoses.

(4) Additional epoxy adhesives were prepared and poured on the microfluidic device to maintain the relative position of the glass capillary tubes and secure well-liquid tightness. Finally, the entire device was placed overnight to completely solidify the epoxy adhesives.

2.3 Experimental setup and manipulation

Before the colloidal emulsion generation experiments, the as-prepared microfluidic device should be sequentially rinsed with alcohol and deionized water for several cycles to eliminate possible residual impurities and then filled the microfluidic chip with deionized water for later use. During the colloidal emulsion generation experiments, syringes loaded with each phase solution were mounted on injection pumps (PHD, PCI 70-3006/70-4501, Harvard Apparatus) and connected to the microfluidic device with Teflon hoses. The activation sequence of the injection pumps followed the rule from the outermost to the innermost fluid phase. During the generation of colloidal double-emulsion droplets, the injection pump corresponding to the middle phase solution started right after the outer phase counterpart and continuously adjusted the flow rate to stably generate colloidal O/W single-emulsion droplets. Afterward, a similar step was implemented to realize a second emulsification with the inner phase solution infusion.

2.4 Characterization

Fig. 1 illustrated the experimental system used to generate and characterize colloidal emulsion droplets. Real-time dynamic droplet generation images were captured using an optical microscope (IX73, Olympus) equipped with a high-speed CCD camera (DP27, Olympus). The acquired data were transmitted and recorded by the supporting software on the connected computer. The produced colloidal emulsion droplets were instantly collected and observed using an optical microscope (BX53, Olympus) equipped with a QImaging Retiga 2000R camera (QImaging, Surrey, Canada). The concentration of colloidal emulsion droplets was determined by calculating the ratio of the droplet volume to total volume. The volume percentage varied from 2.5% v/v to 12.5% v/v for colloidal single-emulsion droplets, and from 3.6% v/v to 33.3% v/v for colloidal double-emulsion droplets during the flow rate regulation experimentas for each phase fluid. Statistical data was then obtained with the assistance of professional image processing software Image J.

3. Results and discussion

As schematically exhibited in Fig. 2, a microfluidic device with a typical flow-focusing configuration can be utilized to prepare colloidal single/double-emulsion droplets in terms of the
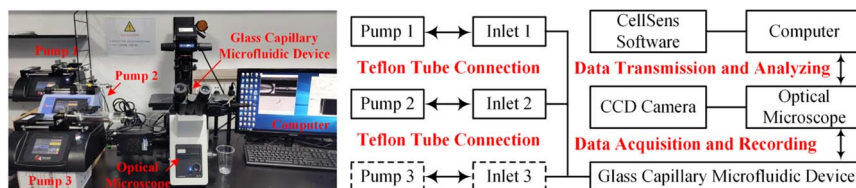
Fig. 1 Experimental and schematic illustration of the system for generating and characterizing colloidal emulsion droplets.

introduction quantities of the fluid phases. In order to facilitate the calculation of geometrical dimensionless parameters, key dimensions of the microfluidic device were abstracted with the D_d and D_c as the diameter of the glass capillary incidence and collection tubes, respectively, where the value D_d was kept identical as 80 μm for all the prepared microfluidic devices. For the preparation of colloidal O/W single-emulsion droplets, the oily fluid Q_1, and the aqueous fluid Q_2 were arranged with a co-flow configuration, which subsequently encountered and emulsified to form droplets with a diameter of D. While for the preparation of colloidal W/O/W double-emulsion droplets, another aqueous fluid Q_3 was introduced to form twice

emulsification to generate core–shell droplets with D_i and D_o as the diameter of the inner core and the outer shell, respectively. For microfluidic devices without the introduction of external physical fields, it was the effect derived from the large-scale flow rate regulation that dominated the generation process of colloidal emulsion droplets. As demonstrated by the generation of colloidal single-emulsion droplets in Fig. 1b, for a microfluidic device with a 300 μm diameter conical glass capillary collection tube and a fixed inner phase flow rate of 0.5 ml h^{-1}, it could be found that the dimension of the generated droplets gradually reduced with respect to the increment of the outer phase flow rate within the squeezing and dripping regime,
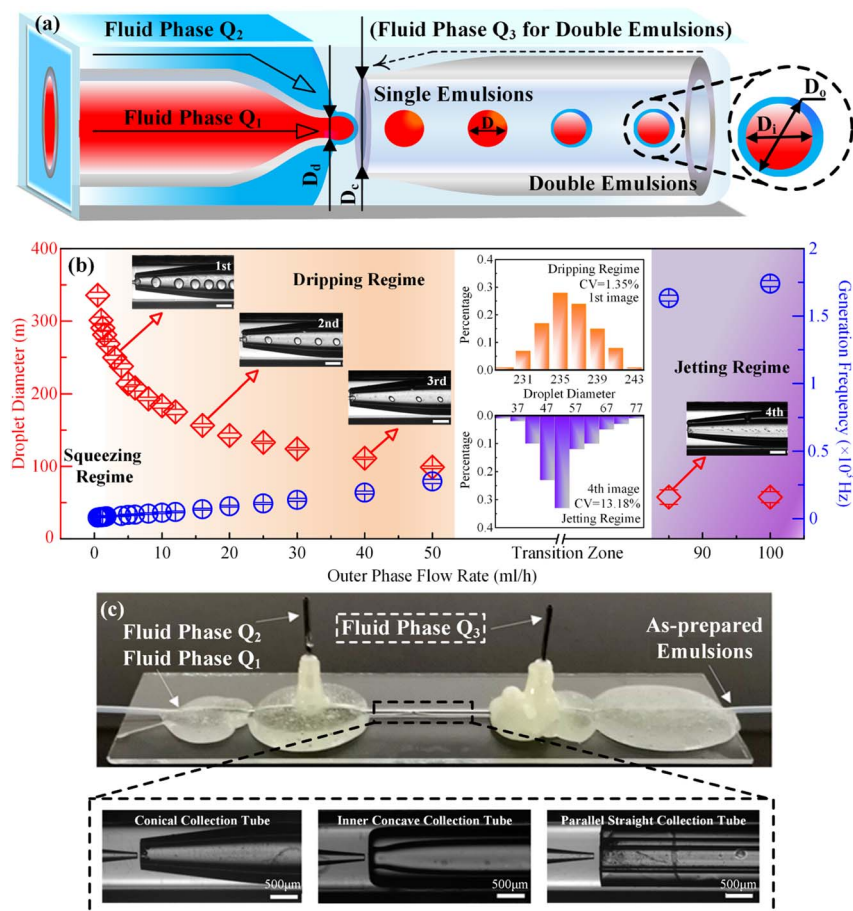

Fig. 2 (a) Schematic illustration of the flow-focusing glass capillary microfluidic device for colloidal single/double-emulsion droplet generation. (b) The microfluidic flow rate regulation results in the generation of colloidal single-emulsion droplets with a traditional conical glass capillary collection tube. (c) The physical illustration of the as-prepared glass capillary microfluidic device with three different morphologies of the collection tube. The scale bars in (b) are 500 μm.
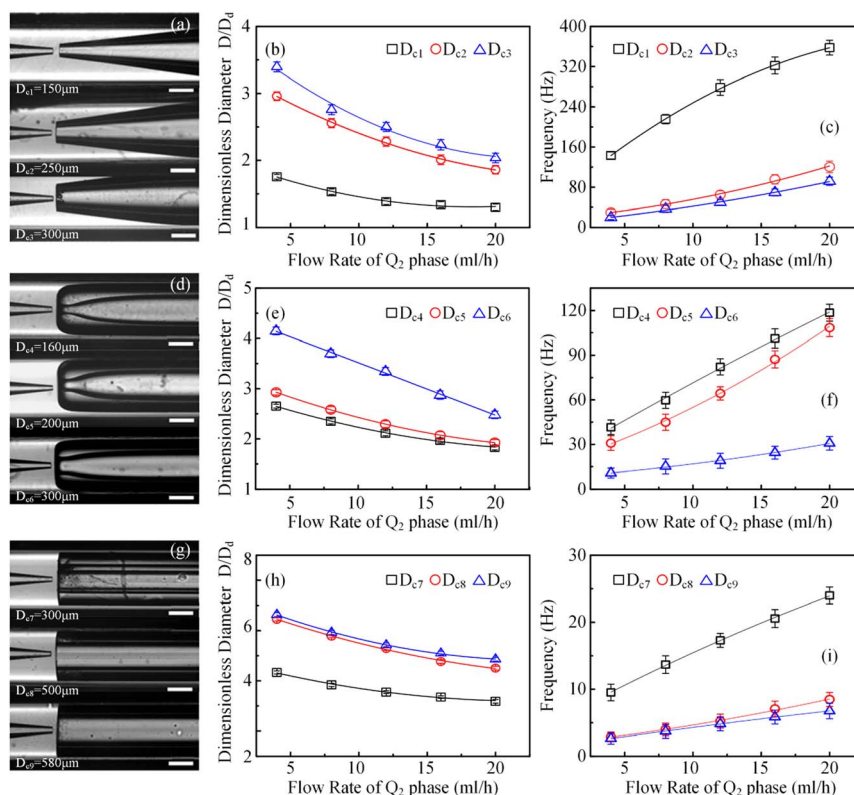
Fig. 3 The integrated regulation results of the generation of colloidal single-emulsion droplets through the combination of flow rate adjustment and the variation of the morphology and the dimension of the collection tubes in glass capillary microfluidic devices. (a) Optical images of microfluidic devices with conical glass capillary collection tubes in three different dimensions. (b) The dimensionless diameters of the colloidal single-emulsion droplets generated with glass capillary microfluidic devices correspond to (a). (c) The generation frequencies of the colloidal single-emulsion droplets produced with glass capillary microfluidic devices correspond to (a). (d) Optical images of microfluidic devices with inner concave glass capillary collection tubes in three different dimensions. (e) The dimensionless diameters of the colloidal single-emulsion droplets generated with glass capillary microfluidic devices correspond to (d). (f) The generation frequencies of the colloidal single-emulsion droplets produced with glass capillary microfluidic devices correspond to (d). (g) Optical images of microfluidic devices with parallel straight glass capillary collection tubes in three different dimensions. (h) The dimensionless diameters of the colloidal single-emulsion droplets generated with glass capillary microfluidic devices correspond to (g). (i) The generation frequencies of the colloidal single-emulsion droplets produced with glass capillary microfluidic devices correspond to (g). In addition, the flow rate of the Q_1 phase is fixed at 0.5 ml h^{-1} during the flow rate regulation of the Q_2 phase. Scale bars are 500 μm.

while the generation frequency exhibited a converse slow growth trend. The generated droplets were quasi-uniform as depicted in the inset images, in which the statistical CV value that corresponds to the first inset image was merely as small as 1.35%. When the outer phase flow rate increased much larger to approximately 85 ml h^{-1}, a regime switch occurred from the dripping to the narrowing jetting due to the overwhelming effect of the viscous drag force exerted by the outer phase fluid over the capillary force. At this moment, the dimension of the droplets decreased even further accompanied by a sharp inflation of the generation frequency, which could be ascribed to the much higher flow rate difference-induced enhanced Rayleigh instability. In addition, the jetting regime rendered the droplets with an inferior monodispersity, as proven by the comparatively larger CV value (13.18%). Although flow rate control was the primary factor in the flow-focusing microfluidic device for colloidal emulsion droplet generation, the morphological and dimensional influence of the glass capillary collection tube could not be ignored. This influence was directly related to the

boundary conditions that altered the viscous shear force to some extent through geometrical confinement, which was still unclear. To clarify this issue, microfluidic devices were fabricated with conical, inner concave, and parallel straight glass capillary collection tubes as shown in Fig. 2c. These devices were used to prepare colloidal emulsion droplets and investigate the relationship between the morphology and dimension of the glass capillary collection tubes and the formation of single-emulsion, single-core double-emulsion, and multi-core double-emulsion droplets.

3.1 Correlations between the glass capillary collection tube variation and the generated colloidal single-emulsion droplets

In order to clarify the influence derived from the glass capillary collection tube variation on the colloidal single-emulsion droplets, nine different microfluidic devices were fabricated, marked from D_{c1} to D_{c9}, which could be classified into three major categories according to the collection tube morphology,
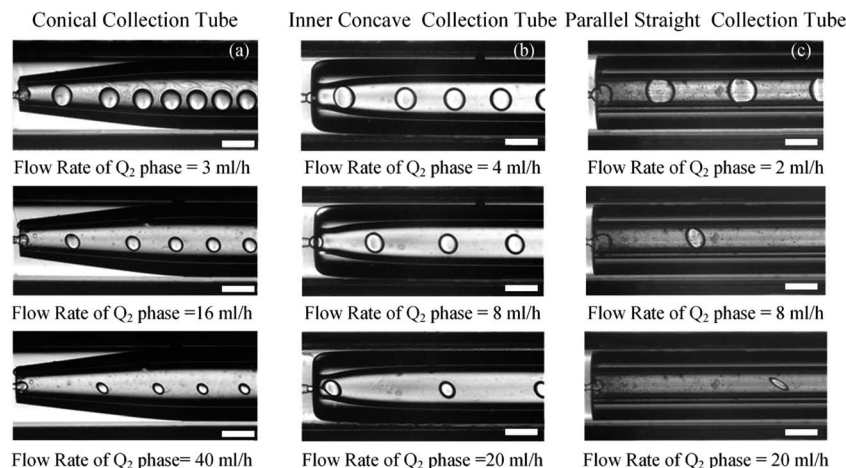
Fig. 4 *In situ* optical images of generated colloidal single-emulsion droplets produced with glass capillary microfluidic devices with three different collection tube morphologies and the same dimension of 300 μm. (a) Optical images of the glass capillary microfluidic device with a conical collection tube. (b) Optical images of the glass capillary microfluidic device with an inner concave collection tube. (c) Optical images of the glass capillary microfluidic device with a parallel straight collection tube. Scale bars are 500 μm.
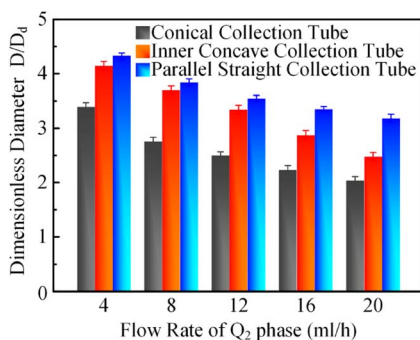
Fig. 5 Dimensionless diameter comparison of the colloidal single-emulsion droplets generated with glass capillary microfluidic devices with the same collection tube dimension, but different collection tube morphologies.

and each category comprised three different dimensions. During the droplet generation process, the inner phase flow rate Q_1 was fixed at 0.5 ml h^{-1}, while the outer phase flow rate Q_2 was gradually increased until the occurrence of the jetting phenomenon. The dimensionless droplet diameter was calculated by dividing the diameter of the glass capillary incidence tube and the corresponding statistical results were shown in Fig. 3. It could be found that the morphological and dimensional variation of the glass capillary collection tube did not affect the overall transformation trend of the dimensionless droplet diameter and the generation frequency. The dimensionless droplet diameter was found to be inversely correlated with the outer phase flow rate due to the enhanced viscous shear force, while the generation frequency showed the opposite trend. The impact of dimensions was uniform and substantial within every major morphological category. The dimensionless diameter of the droplet and the frequency of generation were significantly reliant on the dimensions of the glass capillary collection tube. Specifically, the droplet diameter

was directly proportional and the generation frequency was inversely proportional to the dimensions of the glass capillary collection tube. The dimensionless droplet diameters calculated at different outer phase flow rates were similar when the glass capillary collection tube dimensions were comparable. However, using glass capillary collection tubes with larger dimension discrepancies could significantly affect the dimensionless droplet diameters. This regulation effect was more effective than that derived from large-scale flow rate control. Compared among each major morphological category with an identical glass capillary collection tube dimension of 300 μm, the real-time droplet generation process and the subsequent statistical analysis results were exhibited in Fig. 4, and 5, respectively. Regardless of the variation in outer phase flow rate, the colloidal single-emulsion droplets obtained from the conical glass capillary collection tube were the smallest, whereas the parallel straight glass capillary collection tube generated the largest droplets, and the inner concave glass capillary collection tube produced droplets of intermediate size. Additionally, as the outer phase flow rate increased, the droplet diameter decreased by about 40% in both the conical and inner concave glass capillary collection tubes, with a reduction magnitude around 1.5 times greater than that of the parallel straight glass capillary collection tube. Regarding the flow-focusing effect among the three main morphological categories, it was discovered that the parallel straight glass capillary collection tube had the weakest effect and was the least responsive to changes in the outer phase flow rate. In contrast, the conical glass capillary collection tube showed the opposite trend. Additionally, it was important to note that the inner concave glass capillary collection tube exhibited a distinct combination of characteristics when compared to the other two morphologies. It displayed sensitivity to outer phase flow rate changes and a moderate flow-focusing effect, which could be attributed to its physical configuration. The inner concave morphology preserved both the conical necking feature and the
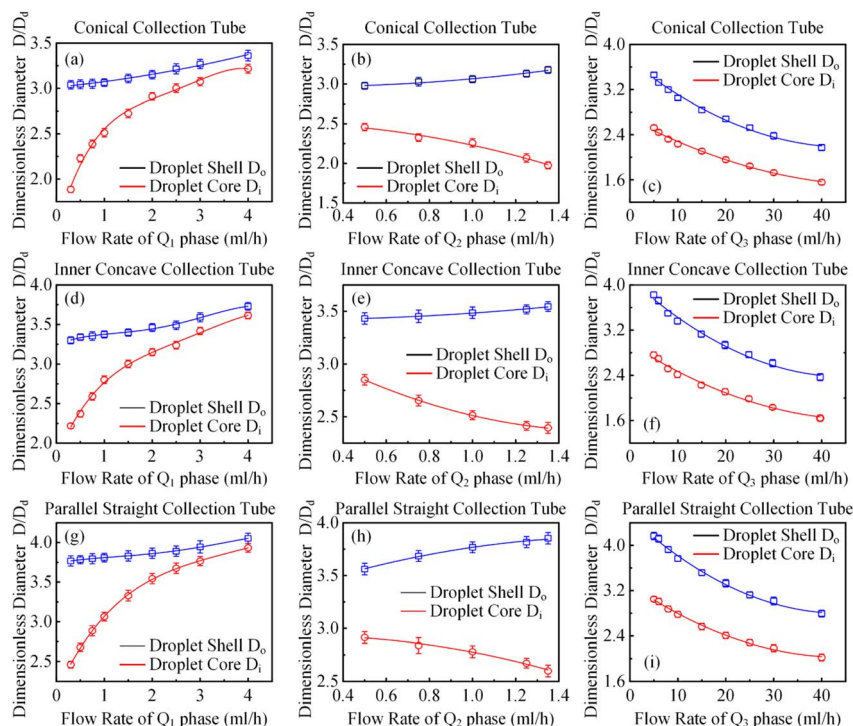
Fig. 6 The integrated regulation results of the generation of colloidal double-emulsion droplets through the combination of three-phase flow rate adjustment and the morphology variation of the collection tubes in glass capillary microfluidic devices. (a–c) Relationships between the dimensionless diameters of the droplet shell D_o and the droplet core D_i of the colloidal double-emulsion droplets concerning the corresponding single-phase flow rate regulation in a glass capillary microfluidic device with a conical collection tube. (d–f) Relationships between the dimensionless diameters of the droplet shell D_o and the droplet core D_i of the colloidal double-emulsion droplets concerning the corresponding single-phase flow rate regulation in a glass capillary microfluidic device with an inner concave collection tube. (g–i) Relationships between the dimensionless diameters of the droplet shell D_o and the droplet core D_i of the colloidal double-emulsion droplets concerning the corresponding single-phase flow rate regulation in a glass capillary microfluidic device with a parallel straight collection tube. In addition, the flow rate of the Q_2 and Q_3 phases are fixed at 1 ml h^{-1} and 10 ml h^{-1} respectively during the flow rate adjustment of the Q_1 phase. The flow rate of the Q_1 and Q_3 phases are fixed at 0.5 ml h^{-1} and 10 ml h^{-1} respectively during the flow rate adjustment of the Q_2 phase. The flow rate of the Q_1 and Q_2 phases are fixed at 0.5 ml h^{-1} and 1 ml h^{-1} respectively during the flow rate adjustment of the Q_3 phase.

larger outer cylindrical ektexine, which occupied most of the square glass capillary tube's internal space. Hence, it could be inferred that the conical necking feature had a significant impact on the droplet diameter response to changes in the outer phase flow rates. Meanwhile, the interstice dimensions between the square glass capillary tube and the collection tube, as well as the conical necking configuration, were the main factors influencing the flow-focusing effect in the production of colloidal single-emulsion droplets. These findings established fundamental principles and provided insights into the efficient control of colloidal single-emulsion droplets through the proper design of glass capillary collection tubes.

3.2 Correlations between the glass capillary collection tube variation and the generated colloidal double-emulsion droplets

It has been demonstrated that altering the glass capillary collection tube could greatly impact the production of colloidal single-emulsion droplets. As the colloidal double-emulsion droplet could be viewed as a higher-order form of the single-emulsion droplet, the resulting influence from the glass

capillary collection tube should be substantial as well. Thus, three microfluidic devices, each with unique glass capillary collection tube morphology but sharing an identical 300 μm orifice dimension, were utilized to generate colloidal double-emulsion droplets by manipulating the flow rates of three-phase fluids. Fig. 6–8 presented the regulation results and the corresponding statistical analysis of the colloidal double-emulsion droplets. The analysis showed that the overall tendency for variation in dimensionless droplet parameters remained unaltered regardless of any variation in the morphology of the glass capillary collection tube. An increased inner phase flow rate was positively associated with an increase in dimensionless diameter for both the droplet core and shell. In all three morphologies, the diameter of the droplet core increased by approximately five times that of the droplet shell, as illustrated in Fig. 7a. Meanwhile, the dimensionless diameter of both the droplet core and shell decreased simultaneously with the increase in the outer phase flow rate due to the enhanced viscous shear force, as demonstrated in Fig. 7c. Furthermore, the dimensionless diameter of the droplet core decreased, while the droplet shell diameter increased as a result of adjusting the flow rate of the middle phase fluid, as shown in
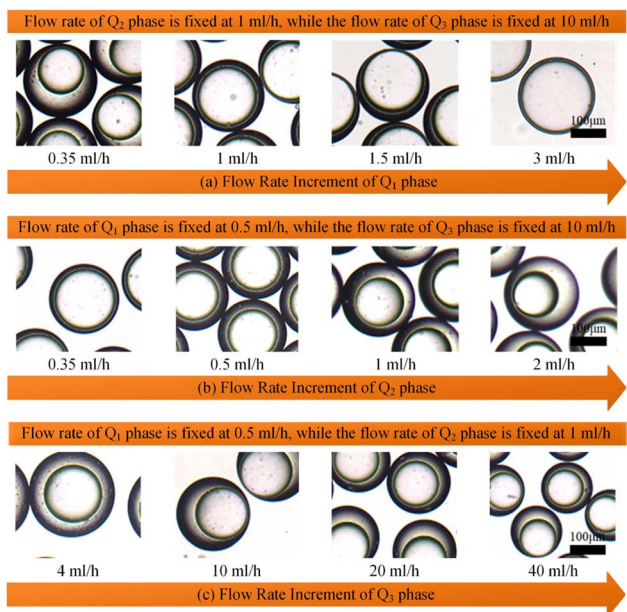
Fig. 7 Optical images of the generated colloidal double-emulsion droplets during the single-phase flow rate adjustment corresponding to Fig. 7(a)–(c), respectively. Scale bars are 100 μm.

Fig. 7b. Although the general trends of the variations appeared similar, there were still certain numerical disparities caused by differences in the morphology of the glass capillary collection tubes. Fig. 8 showed comparative diagrams of the dimensionless diameter of both the core and shell of the colloidal double-emulsion droplet. The largest diameter was consistently observed in the parallel straight glass capillary collection tube, followed by the inner concave glass capillary collection tube, and the smallest diameter was observed in the conical glass capillary collection tube. These observations were consistent regardless of variations in the three-phase flow rate. These results aligned with previous studies on colloidal single-emulsion droplets. Since the fluid interactions in this triphasic flow system were more complex due to the simultaneous presence of two fluid interfaces, the degree of flow-focusing effect that generated colloidal double-emulsion droplets followed a specific order of glass capillary collection tubes: conical,

inner concave, and parallel straight, from largest to smallest. The conical necking design enhanced the flow-focusing effect more effectively than the parallel straight counterpart. Furthermore, it was anticipated to have superior performance in terms of droplet diameter responsiveness to changes in flow rate for each phase. The rule successfully maintained objectivity in terms of the variation of the flow rate of the inner and outer phases. The dimensionless droplet core and shell exhibited a greater variation in magnitude when collected *via* the conical and inner concave glass capillary collection tube, in comparison to the parallel straight glass capillary collection tube, as calculated by percentage. However, a distinct anomaly was observed in the magnitude variation of the droplet shell with respect to the regulation of the flow rate in the middle-phase solution. The magnitude increment for the parallel straight glass capillary collection tube was 8.20%, which was greater than that of the other two glass capillary collection tubes with different morphologies (6.76% for the conical glass capillary collection tube and 3.29% for the inner concave glass capillary collection tube). The reduction in droplet diameter could be attributed to the counteractive effect of regulating the middle-phase solution on both the droplet core and shell. The conical and inner concave glass capillary collection tubes imposed an enhanced viscous shear force during the middle-phase solution regulation, resulting in a remarkable diameter reduction of the droplet core that was approximately 1.5 times greater than that of the parallel straight one. Additional compensation was required in the overall incremental calculation of the droplet shell. This phenomenon differed significantly from the two-phase flow colloidal single-emulsion system. The conical necking configuration in the glass capillary collection tube was again proven advantageous in enhancing the parametric responsiveness of the colloidal droplets to the three-phase flow rate regulation.

Apart from single-core double-emulsion droplets, the double-core and multi-core double-emulsion droplets were also significant constituents of the colloidal double-emulsion droplet family. According to the principles of colloidal single-core double-emulsion droplet generation, delaying the breakup of the middle phase solution should effectively enhance the encapsulation efficiency of core droplets. This could be achieved by indirectly decreasing the flow rate of the
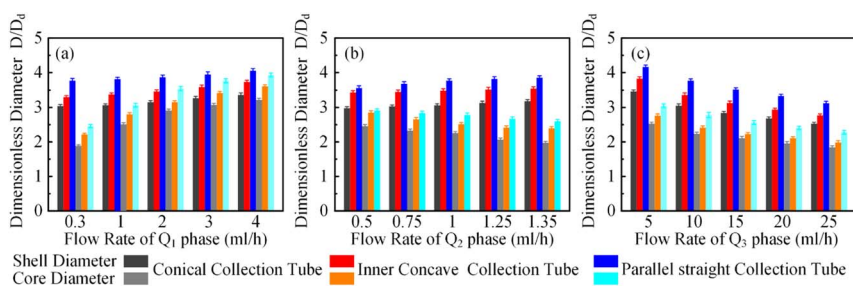

Fig. 8 Statistical analysis of the integrated regulation results of the generation of colloidal double-emulsion droplets through the combination of three-phase flow rate adjustment and the morphology variation of the glass capillary collection tube in microfluidic devices. (a–c) Dimensionless diameter comparison of the colloidal double-emulsion droplets generated with glass capillary microfluidic devices with the same collection tube dimension, but different collection tube morphologies regarding each single-phase flow rate regulation.
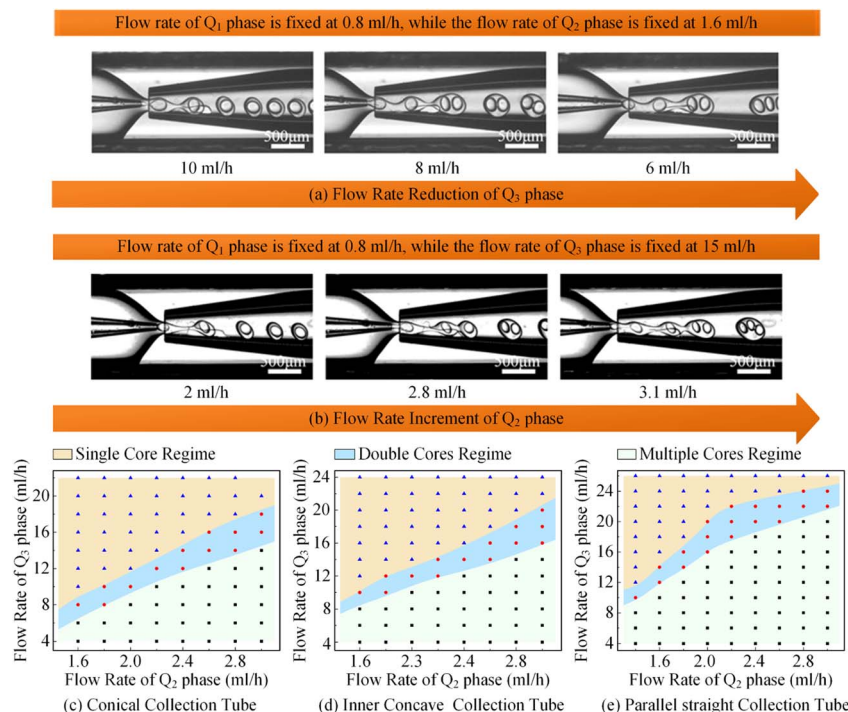
Fig. 9 *In situ* optical images of the generation process of colloidal multicore double-emulsion droplets produced with the glass capillary microfluidic device with a conical collection tube morphology during single-phase flow rate adjustment and the summary of the morphological regime of the colloidal double-emulsion droplets produced by glass capillary microfluidic devices with different collection tube morphologies concerning the flow rate variation of the Q_2 phase and Q_3 phase, while the flow rate of the Q_1 phase is fixed at 0.8 ml h^{-1}. (a) The generation process of colloidal multicore double-emulsion droplets during the single-phase flow rate adjustment of the Q_3 phase. (b) The generation process of colloidal multicore double-emulsion droplets during the single-phase flow rate adjustment of the Q_2 phase. (c) Statistical analysis results of the morphological regime of colloidal double-emulsion droplets generated by the glass capillary microfluidic device with a conical collection tube. (d) Statistical analysis results of the morphological regime of colloidal double-emulsion droplets generated by the glass capillary microfluidic device with an inner concave collection tube. (e) Statistical analysis results of the morphological regime of colloidal double-emulsion droplets generated by the glass capillary microfluidic device with a parallel straight collection tube. Scale bars are 500 μm.

outer phase solution or directly increasing the flow rate of the middle phase solution as demonstrated in Fig. 9a and b, respectively. Thus, the whole morphological regime of the colloidal double-emulsion droplets produced by glass capillary microfluidic devices with different collection tube morphologies could be derived as depicted in Fig. 9c–e. Despite sharing the same dimensions and being regulated under the same flow rate combinations with three-phase fluids, there were significant differences in the morphological distribution regime of the colloidal double-emulsion droplets. When the flow rates of the inner and middle phases were fixed at 0.8 ml h^{-1} and 1.6 ml h^{-1}, respectively, a transition from single-core to double-core double-emulsion droplets occurred as the flow rate of the outer phase decreased to 9 ml h^{-1} for the conical glass capillary collection tube. As the outer phase flow rate was further reduced to 6.5 ml h^{-1}, another transition from double-core to multiple-core double-emulsion droplets took place. Whereas analogous transitions emerged for the inner concave glass capillary collection tube at outer phase flow rates of 10.1 ml h^{-1} and 8.5 ml h^{-1} and for the parallel straight glass capillary collection tube at outer phase flow rates of 14.3 ml h^{-1} and 12 ml h^{-1}. It could be found that the magnitude of the transition flow rates of the outer phase solution was inversely proportional to the flow-

focusing effect of the glass capillary collection tubes. In addition, when the flow rates of the inner and outer phases were set at 0.8 ml h^{-1} and 16 ml h^{-1}, correspondingly, the flow rates of the middle phase associated with the transition from single-core to double-core double-emulsion droplets were observed to be 2.6 ml h^{-1}, 2.4 ml h^{-1}, and 1.8 ml h^{-1} for conical, inner concave, and parallel straight glass capillary collection tubes, the magnitude of which was proportional to the flow-focusing effect of the glass capillary collection tubes. It was plausible to understand that the middle phase solution could be indirectly enhanced by reducing the flow rate of the outer phase solution. Since the stronger flow-focusing effect could improve the dynamic responsivity, this, in turn, required a smaller flow rate of the outer phase solution to balance the intensity disparity in the flow-focusing effect for the conical glass capillary collection tube. Moreover, the enhanced flow-focusing effect would reduce the regulatory impact of directly increasing the flow rate of the middle-phase solution. As a result, a higher flow rate was required for the conical glass capillary collection tube to facilitate the transition from the single-core double-emulsion regime to the multi-core double-emulsion regime, in comparison to the other two morphological glass capillary collection tubes. All the experimental results showed a close correlation

with the variation in the flow-focusing effect caused by different morphologies of the glass capillary collection tubes, and the derived morphological regime of the colloidal double-emulsion droplets could provide a valuable reference for preparing colloidal emulsions, particularly when using flow-focusing glass capillary microfluidic devices.

4. Conclusion

In this study, we experimentally investigated the influence of the geometrical characteristics of glass capillary collection tubes on the generation of colloidal emulsion droplets. Assisted by precise microfabrication technology, glass capillary collection tubes with three distinct morphologies, conical, inner concave, and parallel straight configurations, along with varying orifice dimensions, were prepared and then utilized to fabricate microfluidic devices. Colloidal emulsion droplets were produced under various combinations of flow rates for each phase fluid. The morphological differences of the glass capillary collection tube maintained the basic variation trend of droplet parameters during the flow rate regulation process. However, discrepancies in the flow-focusing effect were found to cause certain numerical differences. The size of the orifice in the glass capillary collection tube had a significant impact on the colloidal emulsion droplets. A smaller orifice reduced the dimension and improved the generation frequency of colloidal emulsion droplets. The morphology differences resulted in a discrepancy in the flow-focusing effect, which followed a sequence from largest to smallest: conical, inner concave, and parallel straight configurations. The presence of a conical necking structure and a larger gap between the square glass capillary tube and the glass capillary collection tube enhanced the flow-focusing effect. Therefore, the droplets produced by the conical glass capillary collection tube were consistently the smallest. Additionally, the conical glass capillary collection tube required a lower outer phase flow rate and a higher middle phase flow rate to achieve the transition from single-core to multi-core double-emulsion droplets during the single-phase flow rate regulation. These experimental results provided guidance and qualitative instructions for regulating the flow-focusing effect in glass capillary microfluidic devices, facilitating the preparation of desired colloidal emulsion droplets.

Author contributions

This paper was written through the contributions of all authors and the specific contributions were listed as follows: supervision, resources, revision, project administrator, and funding acquisition (T. J.); conceptualization, methodology, investigation, experimentation, original drafting, revision, editing (H. W.); investigation, revision (S. L.); investigation, supervision, resources (H. Y.); supervision, funding acquisition, resources (H. J.). All authors have approved the final version of the manuscript.

Conflicts of interest

There are no conflicts to declare.

Acknowledgements

References

1 X. Chen, L. Hou, Z. Zhang, R. Lin, R. Lin, C. Yan and F. Bao, *Colloids Surf., A*, 2022, **655**, 130227.

2 Y. Jia, Y. Ren, W. Liu, L. Hou, Y. Tao, Q. Hu and H. Jiang, *Lab Chip*, 2016, **16**, 4313–4318.

3 Y. Jia, Y. Ren, L. Hou, W. Liu, T. Jiang, X. Deng, Y. Tao and H. Jiang, *Lab Chip*, 2018, **18**, 1121–1129.

4 Y. Jia, Y. Ren, L. Hou, W. Liu, X. Deng and H. Jiang, *Small*, 2017, **13**, 1702188.

5 C. Zhou, P. Zhu, X. Han, R. Shi, Y. Tian and L. Wang, *Lab Chip*, 2021, **21**, 2684–2690.

6 Q. Fan, Y. Guo, S. Zhao and B. Bao, *RSC Adv.*, 2022, **12**, 20686–20695.

7 H. Sun, Y. Ren, Y. Tao, W. Liu, T. Jiang and H. Jiang, *Sens. Actuators, B*, 2020, **304**, 127397.

8 X. Deng, Y. Ren, L. Hou, W. Liu, Y. Jia and H. Jiang, *ACS Appl. Mater. Interfaces*, 2018, **10**, 40228–40237.

9 X. Deng, Y. Ren, L. Hou, W. Liu, T. Jiang and H. Jiang, *Small*, 2019, **15**, e1903098.

10 K. Zhu, Y. Yu, Y. Cheng, C. Tian, G. Zhao and Y. Zhao, *ACS Appl. Mater. Interfaces*, 2019, **11**, 4826–4832.

11 L. Shang, Y. Cheng, J. Wang, Y. Yu, Y. Zhao, Y. Chen and Z. Gu, *Lab Chip*, 2016, **16**, 251–255.

12 D. Chong, X. Liu, H. Ma, G. Huang, Y. L. Han, X. Cui, J. Yan and F. Xu, *Microfluid. Nanofluid.*, 2015, **19**, 1071–1090.

13 X. Zhao, F. Bian, L. Sun, L. Cai, L. Li and Y. Zhao, *Small*, 2020, **16**, e1901943.

14 M. Wu, S. Wu, G. Wang, W. Liu, L. T. Chu, T. Jiang, H. K. Kwong, H. L. Chow, I. W. S. Li and T.-H. Chen, *Sci. Adv.*, 2022, **8**, eabn6064.

15 L. Hou, Z. Liang, X. Fan, J. Yu and F. Bao, *Sens. Actuators, B*, 2023, **394**, 134344.

16 H. Wu, Y. Ren, T. Jiang, J. Chen, W. Wu, Y. Lu and H. Jiang, *Int. J. Appl. Ceram. Technol.*, 2022, **19**, 2979–2989.

17 X. Deng, Y. Ren, L. Hou, T. Jiang and H. Jiang, *Lab Chip*, 2021, **21**, 1517–1526.

18 K. Zhang, Y. Ren, T. Jiang and H. Jiang, *Anal. Chim. Acta*, 2021, **1182**, 338955.

19 B. G. Chung, K. H. Lee, A. Khademhosseini and S. H. Lee, *Lab Chip*, 2012, **12**, 45–59.

20 Y. Liu, *RSC Adv.*, 2019, **9**, 17623–17630.

21 S. Zhang, T. Jiang, F. Han, L. Cao, M. Li, Z. Ge, H. Sun, H. Wu, W. Wu, N. Zhou, M. L. Akhtar and H. Jiang, *Chem. Eng. J.*, 2024, **480**, 148347.

22 H. Wu, J. Chen, T. Jiang, W. Wu, M. Li, S. Zhang, Z. Li, H. Ye, M. Zhu, J. Zhou, Y. Lu and H. Jiang, *Micromachines*, 2024, **15**(1), 109.

23 W. M. Hamonangan, S. Lee, Y. H. Choi, W. Li, M. Tai and S.-H. Kim, *ACS Appl. Mater. Interfaces*, 2022, **14**, 18159–18169.

24 Y. Matsuura-Sawada, M. Maeki, T. Nishioka, A. Niwa, J. Yamauchi, M. Mizoguchi, K. Wada and M. Tokeshi, *ACS Appl. Nano Mater.*, 2022, **5**, 7867–7876.

25 N. Hu, K. Cheng, S. Zhang, S. Liu, L. Wang, X. Du, Y. Li and C. Li, *Analyst*, 2023, **148**, 1653–1671.

26 D. Park, H. Kim and J. W. Kim, *Biomicrofluidics*, 2021, **15**, 051302.

27 P. Zhu and L. Wang, *Chem. Rev.*, 2022, **122**, 7010–7060.

28 H. Wu, Y. Ren, T. Jiang, W. Wu, Y. Lu and H. Jiang, *Lab Chip*, 2022, **22**, 836–847.

29 H. Wu, T. Jiang, W. Wu, S. Zhang, M. Li, J. Zhou, M. Zhu, J. Chen, Z. Li, Y. Lu and H. Jiang, *Colloids Surf., A*, 2023, **677**, 132428.

30 J. M. Montanero and A. M. Ganan-Calvo, *Rep. Prog. Phys.*, 2020, **83**, 097001.

31 J. Eggers and E. Villermaux, *Rep. Prog. Phys.*, 2008, **71**, 036601.

32 A. S. Utada, A. Fernandez-Nieves, H. A. Stone and D. A. Weitz, *Phys. Rev. Lett.*, 2007, **99**, 094502.

33 A. S. Utada, A. Fernandez-Nieves, J. M. Gordillo and D. A. Weitz, *Phys. Rev. Lett.*, 2008, **100**, 014502.

34 T. Glawdel and C. L. Ren, *Phys. Rev. E*, 2012, **86**, 026308.

35 R. Xue, W. Liu, T. Jiang, C. Song, H. Jiang and Y. Ren, *Adv. Mater. Interfaces*, 2020, **7**, 2000345.

36 P. Zhu and L. Wang, *Lab Chip*, 2016, **17**, 34–75.

37 P. Zhu, T. Kong, X. Tang and L. Wang, *Nat. Commun.*, 2017, **8**, 15823.

38 F. Tu and D. Lee, *J. Am. Chem. Soc.*, 2014, **136**, 9999–10006.

39 S. Park, S. S. Lee and S. H. Kim, *Adv. Mater.*, 2020, **32**, e2002166.

40 H. Zhang, W. Cui, X. Qu, H. Wu, L. Qu, X. Zhang, E. Makila, J. Salonen, Y. Zhu, Z. Yang, D. Chen, H. A. Santos, M. Hai and D. A. Weitz, *Proc. Natl. Acad. Sci. U. S. A.*, 2019, **116**, 7744–7749.

41 M. Michelon, Y. Huang, L. G. de la Torre, D. A. Weitz and R. L. Cunha, *Chem. Eng. J.*, 2019, **366**, 27–32.

42 X.-H. He, W. Wang, K. Deng, R. Xie, X.-J. Ju, Z. Liu and L.-Y. Chu, *RSC Adv.*, 2015, **5**, 928–936.

43 P. Zhu, R. Chen, C. Zhou, M. Aizenberg, J. Aizenberg and L. Wang, *Adv. Mater.*, 2021, **33**, 2008558.

44 C. Zhou, P. Zhu, Y. Tian, M. Xu and L. Wang, *ACS Nano*, 2019, **13**, 6319–6329.

45 M. Zou, J. Wang, Y. Yu, L. Sun, H. Wang, H. Xu and Y. Zhao, *ACS Appl. Mater. Interfaces*, 2018, **10**, 34618–34624.

46 X. Y. Du, Q. Li, G. Wu and S. Chen, *Adv. Mater.*, 2019, **31**, e1903733.

47 C. X. Zhao, D. Chen, Y. Hui, D. A. Weitz and A. P. J. Middelberg, *Chemphyschem*, 2017, **18**, 1393–1399.

48 L. Hou, H. Jiang and D. Lee, *Chem. Eng. J.*, 2016, **288**, 539–545.

49 J.-Y. Kwon, M. Khan and S.-Y. Park, *RSC Adv.*, 2016, **6**, 55976–55983.

50 J. Park, S. S. Lee, Y. H. Sohn, S.-H. Kim and Y. Seo, *RSC Adv.*, 2016, **6**, 85012–85018.

51 L. Shang, Y. Cheng and Y. Zhao, *Chem. Rev.*, 2017, **117**, 7964–8040.

52 C. L. Mou, W. Wang, Z. L. Li, X. J. Ju, R. Xie, N. N. Deng, J. Wei, Z. Liu and L. Y. Chu, *Adv. Sci.*, 2018, **5**, 1700960.

53 W. Li, L. Zhang, X. Ge, B. Xu, W. Zhang, L. Qu, C. H. Choi, J. Xu, A. Zhang, H. Lee and D. A. Weitz, *Chem. Soc. Rev.*, 2018, **47**, 5646–5683.

54 J. Qi, X. Lai, J. Wang, H. Tang, H. Ren, Y. Yang, Q. Jin, L. Zhang, R. Yu, G. Ma, Z. Su, H. Zhao and D. Wang, *Chem. Soc. Rev.*, 2015, **44**, 6749–6773.

55 W.-T. Wang, R. Chen, J.-H. Xu, Y.-D. Wang and G.-S. Luo, *RSC Adv.*, 2014, **4**, 16444.

56 H. Wu, Y. Ren, L. Hou, T. Jiang and H. Jiang, *Lab Chip*, 2020, **20**, 4600–4610.